Dynamics and Control of a Buoyancy-Driven Underwater Vehicle for Estimating and Tracking the Scattering Layer

Rachel J. Suitor[1], Eric Berkenpas[2], and Derek A. Paley[3]

***Abstract*—This paper presents the design of a control strategy for an autonomous buoyancy-driven underwater vehicle, called the Driftcam, tasked with estimating and tracking the pelagic acoustic-scattering layer at depths of up to 700 meters. This reference-tracking control design is an alternative to the onboard control currently implemented on the Driftcam, as the existing control architecture is not designed for time-varying setpoint tracking. Tracking a known reference is presented using state-feedback control for continuous- and discrete-time command inputs. The known reference signal is chosen to represent the pelagic scattering layer vertical migration dynamics, modeled as a simple harmonic oscillator and estimated with a dynamic observer. We define a measurement function for the depth-varying density of organisms observable in the scattering layer. Time-varying reference tracking control is presented using output feedback for continuous- and discrete-time command inputs, where the reference is the online position estimate of the scattering layer. We also present an offboard trajectory motion planning algorithm using the existing onboard controller to emulate the response of the proposed reference tracking strategy. Experimental results from laboratory and field testing of the trajectory motion planner demonstrate that the buoyancy engine can feasibly achieve the desired behavior of the reference-tracking control strategy.**

***Index Terms*—Marine robotics, underactuated robots, nonlinear dynamics, motion planning and control**

I. Introduction

THE National Geographic Driftcam is a robotic imaging platform, pictured in Fig. 1a, with buoyancy-driven depth control used to study the deep-water pelagic scattering layer. The acoustic-scattering layer is a pelagic ecosystem consisting of marine organisms that exhibit diel vertical migration, following zooplankton up through the water column to feed at shallow depths during the night [1]. This ecosystem is the largest on the planet in terms of biomass and number of individual organisms and is dense enough to be observed by sonar from surface vessels using an echosounder [1], [2]. While detail on specific species within the scattering layer can be obtained by deploying a tethered echosounder at depth to count and measure individual organisms [3], sonar alone is not sufficient to make definitive conclusions about the community structure and behavior within the layer. In some cases there may be strong correlation between animal species observed visually from an *in situ* platform and an acoustically defined scattering layer [4], [5]. Additionally, there may be assemblages that can be observed visually but not detectable by sonar [6]. An optical *in situ* platform like Driftcam, which is equipped with a high definition low-light video camera (Fig. 1b), can provide vital complementary data when deployed simultaneously with ship-based active acoustics.

Underwater vehicles often require difficult-to-design control systems due to the nonlinear nature of their dynamics and uncertain models of the underwater environment. Controllers for underwater vehicles often focus on attitude control, resulting in overactuated vehicles with multiple thrusters [8], [9]. However, thrusters are disruptive to the pelagic ecosystem, which makes it difficult to observe the natural behavior of the scattering layer [5]. Techniques for imaging pelagic scattering layer ecosystems typically use manned submersibles [4], [10], [11], remotely operated vehicles [11]–[14] or autonomous underwater vehicles [15]–[18]. Lagrangian floats employing active buoyancy control have been employed globally for ocean chemistry measurements and are optimized for low payload and long endurance [19]. Robotic floats have been fitted with cameras for pelagic surveys [19] and seafloor surveys [20]. The Driftcam was developed as an alternative to these technologies providing a unique combination of payload capacity, a large battery system, high-performance cameras, powerful lights, ease of deployment, recoverability, and cost. It is a robotic float that is buoyancy controlled and passively stable in vertical orientation [21], [22].

Prior work developed the Driftcam vehicle and buoyancy engine, focusing on station-keeping depth control [5], [7]. In this paper, we expand on our prior work by introducing an estimation and control strategy for Driftcam to track a time-varying reference that represents the scattering layer and a trajectory-planning algorithm for automated operation.

The technical approach is to design complementary onboard control and offboard guidance of the Driftcam vehicle based on a dynamic model of a single particle with two degrees of freedom. We design a control strategy for nonlinear reference tracking using an error-based method [23] in continuous and

Manuscript received: October 4, 2022; Revised: January 31, 2023; Accepted March 8, 2023.

This paper was recommended for publication by Editor P. Pounds upon evaluation of the Associate Editor and Reviewers' comments. R. Suitor was supported by the National Geographic Society and the Link Foundation. E. Berkenpas was supported by the Department of the Navy, Office of Naval Research.

[1]Rachel J. Suitor is with the Department of Aerospace Engineering, University of Maryland, College Park, MD 20740, USA rjsuitor@umd.edu

[2]Eric Berkenpas is with Second Star Robotics LLC, Silver Spring, MD 20910, USA eric@secondstarrobotics.com

[3]Derek A. Paley is with the Department of Aerospace Engineering and the Institute for Systems Research at the University of Maryland, College Park, MD 20740, USA dpaley@umd.edu

Digital Object Identifier (DOI): see top of this page.

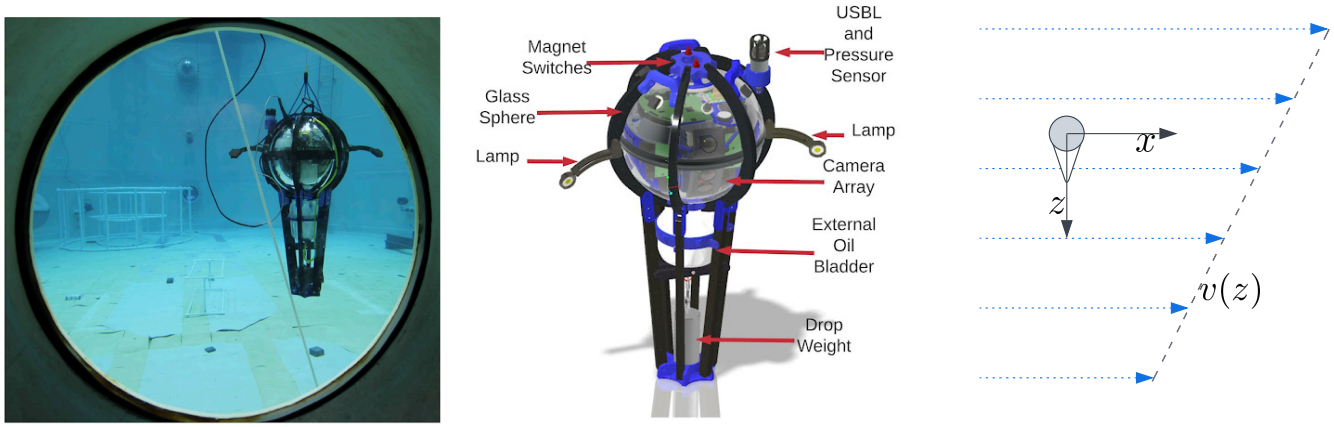

(a) (b) (c)

Fig. 1. (a) Driftcam in the Neutral Buoyancy Research Facility at the University of Maryland [7]; (b) Driftcam's major components [7]; (c) position coordinates.

discrete time. Furthermore, we use an estimation strategy with the scattering layer dynamics to track a time-varying reference representing the scattering layer depth, to simulate a layer depth observed with an echo sounder or cameras in a controlled manner. This work lays the groundwork for autonomous operation of the Driftcam using onboard measurements with minimum reliance on the surface vessel. Continuous communication between the surface vessel and the Driftcam interferes with the data collection of the ship's echosounder. Therefore, contact with the surface vessel is limited to intermittent feedback control inputs sent to the vehicle at discrete time intervals through a low-bandwidth acoustic link. This intermittent control strategy is also applicable to underactuated robotic systems in air and space domains.

The specific contributions of this paper are (1) a strategy for state- or output-feedback control to track a time-varying reference signal by adjusting the vehicle's depth using continuous- or discrete-time updates; and (2) an offboard guidance strategy that utilizes the low-bandwidth acoustic communication between the surface vessel and Driftcam to implement the reference-tracking algorithm without modifying the existing onboard controller. The onboard controller is designed to decrease reference-tracking error, whereas the offboard guidance is designed to increase automation and overall autonomy of the system. Such an increase in autonomy is necessary for deployment of multiple Driftcams where it becomes prohibitively difficult for human operators to monitor and control multiple vehicles simultaneously. The offboard guidance framework allows new software to be tested offshore with reduced risk by allowing a human-in-the-loop. Simulation results demonstrate convergence of the proposed control strategy. Simulation and experimental results, including sea trials near Bermuda, demonstrate the closed-loop response of the vehicle as configured in [5] and [7].

The outline of the paper is as follows. Section II describes the dynamics of the Driftcam vehicle and a model for the scattering layer dynamics. Section III presents and analyzes a theoretical strategy for tracking a time-varying reference. Section IV presents the automatic trajectory planner and experimental results from laboratory and field testing. Section V summarizes the paper and ongoing work.

II. System Background

A. Platform Description

The Driftcam (Fig. 1b) is an isobaric robotic float containing an electrically actuated pump driven by a high-torque stepper motor. Like most commercially available profiling floats, the Driftcam utilizes a reciprocating pump for oil displacement [24]. The engine transfers mineral oil from a 2-liter reservoir inside a spherical glass pressure housing to an external oil bladder to effect volume adjustment. The pump is controlled by a low-power 16-bit microcontroller that utilizes a commercially available pressure-based sensor that applies a linear conversion based on a simplification of the Saunders and Fofonoff method [25] to provide depth feedback. In addition to the pressure sensor, the platform includes a temperature sensor, attitude sensors, and a camera array. An embedded Linux computer enables image capture and real-time processing of frames from the camera array. Two LED lamps provide artificial lighting for the camera array and strobe on the surface. A drop weight released by a burn-wire is used to reduce ballast in the event of a system failure. An integrated VHF and Iridium beacon is used to aid surface localization and recovery. A more detailed description of the electrical and mechanical design of the Driftcam can be found in [7].

B. Driftcam dynamics and control

This section describes an idealized model of the dynamics and onboard control of the Driftcam, presents laboratory experimental results for onboard control, and describes a simplified model for the scattering layer migration dynamics.

During dives, the Driftcam is trimmed to be neutrally buoyant at deployment and can achieve a maximum vertical speed of approximately 20 cm/s [7]. Nominally, the maximum operational speed is constrained to 12 cm/s. Because of the nonlinear relationship between terminal velocity and buoyancy correction, the velocity limitation simplifies the control problem by constraining it. The 12 cm/s limit is also greater than

diel vertical migration rates found in nature, which typically do not exceed 8.7 cm/s [26].

Consider a particle model of the motion of an underwater vehicle with buoyancy control subject to horizontal currents. Let $(x, z, \dot{z})$ denote the horizontal position, vertical depth (positive down), and vertical descent rate of the vehicle, shown in Fig. 1c. The horizontal current, which may depend on the vehicle's depth, is denoted by $v = v(z)$. Assume the vehicle's motion in the horizontal direction is equal to the speed of the current. The vehicle's motion in the vertical direction is subject to hydrodynamic drag. Let b denote the specific hydrodynamic drag coefficient. The quadratic drag coefficient and vehicle mass were determined experimentally to be 208.456 kg/m and 54.665 kg, respectively. The equations of motion are

$$\dot{x} = v \tag{1}$$
$$\ddot{z} = \mathrm{sat}(\mu) - b\dot{z}|\dot{z}|, \tag{2}$$

where $\mu = \mu(x, z, \dot{z})$ denotes the specific force control effort, which is the difference between the vehicle buoyancy and gravity. The saturation function, $\mathrm{sat}(\mu)$ [23] constrains the input range to $\mu \in [-\mu_{\max},\ \mu_{\max}]$ as limited by the vehicle's finite capacity to regulate its buoyancy, where $\mu_{\max}$ denotes the maximum vertical specific force.

The particle model is an idealized description of the Driftcam dynamics and does not account for all of the forces and phenomena that govern the motion of a buoyancy controlled robotic float. Sources of model inaccuracy include vehicle mass, added mass, ocean density stratification, vehicle compressibility, vehicle thermal expansion, and buoyancy engine flow accuracy [27]. Despite lacking fidelity, the idealized model is a useful compromise between accuracy, computation time, and the effort needed to perform system identification.

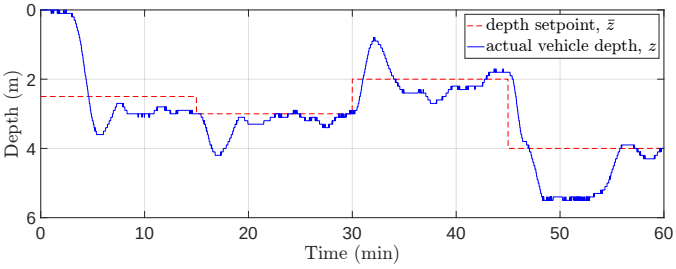

Fig. 2. Laboratory experimental results of existing onboard depth control from Driftcam pool testing for a specific depth profile.

The change in volume, and thus buoyancy, is regulated onboard the Driftcam by a PID feedback control law [5]. The depth of the vehicle is driven to the desired depth setpoint by PID feedback control with depth and velocity states estimated using a Kalman filter. Laboratory experimental results demonstrate the closed-loop response of the Driftcam using the onboard PID control and state estimation to achieve a specific setpoint [7]. The pool test results in Fig. 2 show the vehicle response for a one-hour test dive given four setpoints commanded at uniform intervals of 15 minutes. Trapped air in the Driftcam frame produces depth control instability near the surface as gas bubbles rapidly increase buoyancy near the surface and decrease buoyancy at depth. Overshoot after depth transitions is thought to be associated with this effect. The root-mean-squared error is within 1 meter, which is acceptable for targeting scattering layer ecosystems.

C. Scattering layer migration dynamics

The dynamics of the scattering layer nominal depth ζ are modeled as a second-order oscillator representing the daily vertical migration of the pelagic ecosystem [1]

$$\ddot{\zeta} = -\omega_0^2(\zeta - \zeta_0), \tag{3}$$

where ζ is the scattering layer depth and ω_0 and ζ_0 are the natural frequency and amplitude of the scattering layer dynamics, respectively. To estimate the nominal depth of the scattering layer, a dynamic observer is introduced to the system with a measurement that represents the activity level of marine organisms in the field of view of an onboard camera.

The measurement of interest is the scalar count of visible organisms at a particular depth, which is obtained through onboard image processing. The number of organisms is highest at the scattering layer nominal depth and drops off outside some vertical thickness $\eta = \eta(\zeta)$, which varies with the depth of the layer. For simplicity, assume that the total number of organisms present remains the same, while the vertical spread of the layer expands and contracts with increasing and decreasing depth, respectively (illustrated in [7, Fig. 10]). To represent this variation in the observation function we include a scaling parameter $\gamma = \gamma(\zeta)$ that also varies with the scattering layer nominal depth.

The scattering layer observation is modeled as a Gaussian bump function:

$$y(\zeta, z) = \begin{cases} \gamma(\zeta)\exp\left(\frac{-1}{\eta(\zeta)^2 - |\zeta - z|^2}\right), & \text{if } |\zeta - \mathrm{z}| < \eta \\ 0, & \text{otherwise.} \end{cases} \tag{4}$$

The scattering layer thickness varies linearly with depth, i.e., $\eta(\zeta) = c_\eta\zeta + \eta_0$, where c_η is the rate of change with depth and η_0 is the minimum thickness of the layer. The scaling parameter γ represents the maximum number of targets counted at a particular depth and decreases as the layer thickness increases, i.e., $\gamma(\zeta) = c_\gamma\zeta + \gamma_0$, where c_γ is the rate of change with depth and γ_0 is the maximum scaling parameter.

III. Control Design for Onboard Reference Tracking

This section presents a design for an onboard error-based reference tracking controller with known and estimated references signals in either continuous or discrete time. The proposed control strategy lays the groundwork for fully autonomous monitoring of the pelagic scattering layer using a buoyancy-driven vehicle with minimal reliance on a surface vessel.

A. Tracking a known reference

This section presents continuous- and discrete-time control strategies for tracking a known reference signal with the

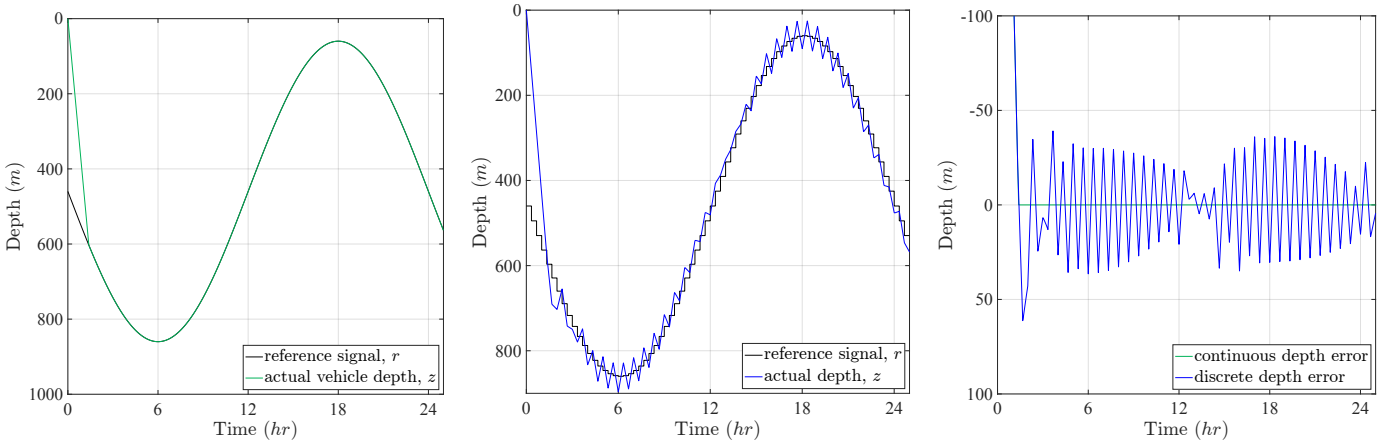

Fig. 3. Simulated state-feedback reference tracking: (a) continuous-time reference tracking; (b) discrete-time reference tracking with a 20-minute update interval; (c) tracking error

Driftcam. The reference signal $r(t)$ represents the oscillatory motion of the layer as a function of time t, given by

$$r(t) = \zeta_0(1 + \sin(\omega_0 t)) + r(0). \tag{5}$$

Note that (5) is a solution to (3). The reference tracking strategy follows a control method in which the tracking error is defined with respect to a known reference signal and its bounded derivatives, following [23]. Feedback linearization is used to handle the nonlinearities present in the error dynamics. The continuous-time error dynamics are proven to be exponentially stable. For discrete-time reference tracking, the error dynamics has a nonvanishing perturbation. Lemma 9.2 in [23] establishes the stability of the discrete-time error dynamics.

Continuous-time reference tracking: For continuous-time reference tracking with Driftcam, the depth setpoints used in the existing controller (previously described in Section II-B) are now defined to be the continuous reference signal $r(t)$ in (5), which is assumed to be available from the surface vessel. In practice, the reference signal used for ground truth would be generated by ship-based observations (e.g. from an echosounder). The continuous-time depth dynamics are given in (2), where the system output is z. The tracking error is denoted as $\mathbf{e} = [e_1\ e_2]^T$, where $e_1 = z - r$ and $e_2 = \dot{z} - \dot{r}$ [23]. The continuous-time error dynamics are

$$\dot{e}_1 = e_2 \tag{6}$$
$$\dot{e}_2 = \ddot{z} - \ddot{r} = \mu - b\dot{z}|\dot{z}| - \ddot{r}. \tag{7}$$

The error-based tracking control input μ is chosen to linearize (7) with state feedback such that the error dynamics can be written in the linear form $\dot{\mathbf{e}} = (\mathbf{A} - \mathbf{BK})\mathbf{e}$ where

$$\mathbf{A} = \begin{bmatrix} 0 & 1 \\ 0 & 0 \end{bmatrix} \text{ and } \mathbf{B} = \begin{bmatrix} 0 \\ 1 \end{bmatrix}. \tag{8}$$

The gains $\mathbf{K} = [K_1,\ K_2]$ are chosen to place the poles of $\mathbf{A} - \mathbf{BK}$ in the open left-half complex plane.

Assume $|\mu| < \mu_{\max}$, which implies

$$\mu = b\dot{z}|\dot{z}| + \ddot{r} - K_1 e_1 - K_2 e_2. \tag{9}$$

Substituting (9) into (7), yields

$$\dot{e}_2 = -K_1 e_1 - K_2 e_2. \tag{10}$$

The tracking error dynamics (6) and (10) exponentially stabilize the origin $\mathbf{e} = 0$. The vehicle converges to the desired reference as shown in Fig. 3a, with initial conditions $z(0) = 0$ and $r(0) = \zeta_0$, and manually tuned gains $K_1 = 2$ and $K_2 = 3$. The depth converges to the desired trajectory in approximately 84 minutes. The dynamics are integrated for one full period of the scattering layer migratory oscillation, i.e., 24 hours.

In the case that the control μ reaches the saturation limit $\mu_{\max}$, then

$$\mu = \text{sgn}(\mu)\mu_{\max} \tag{11}$$
$$= b\dot{z}|\dot{z}| + \ddot{r} - K_1 e_1 - K_2 e_2 + \delta \tag{12}$$

where $\delta = \text{sgn}(\mu)\mu_{\max} - (b\dot{z}|\dot{z}| + \ddot{r} - K_1 e_1 - K_2 e_2)$ is the difference between the saturation limit and the desired control. Substituting (12) into (7), yields

$$\dot{e}_2 = -K_1 e_1 - K_2 e_2 + \delta. \tag{13}$$

Since $|\delta| \to 0$ as $\|\mathbf{e}\| \to 0$ for all $t \geq 0$, the system satisfies Lemma 9.1 [23]. Therefore, δ is a vanishing perturbation and the origin $\mathbf{e} = 0$ remains exponentially stable.

Discrete-time reference tracking: The USBL on the Driftcam is broadband in nature and shares an acoustic frequency with many ship-based echosounders. While the Driftcam is communicating, the ship-based echosounder cannot resolve backscatter. Because echosounder data is generally collected continuously, it was agreed to communicate with the Driftcam for 3 seconds no more than once every 5 minutes. Reduced updates from the Driftcam require discrete-time reference tracking. By discretizing the control strategy, we reach a feasible solution with command updates transmitted intermittently to the acoustic modem on the Driftcam. Interference to the echosounder is minimal if command updates are sent at regular intervals of at least 5–10 minutes [7].

To adapt the continuous-time analysis of the error-based tracking control in the previous section to discrete-time, each

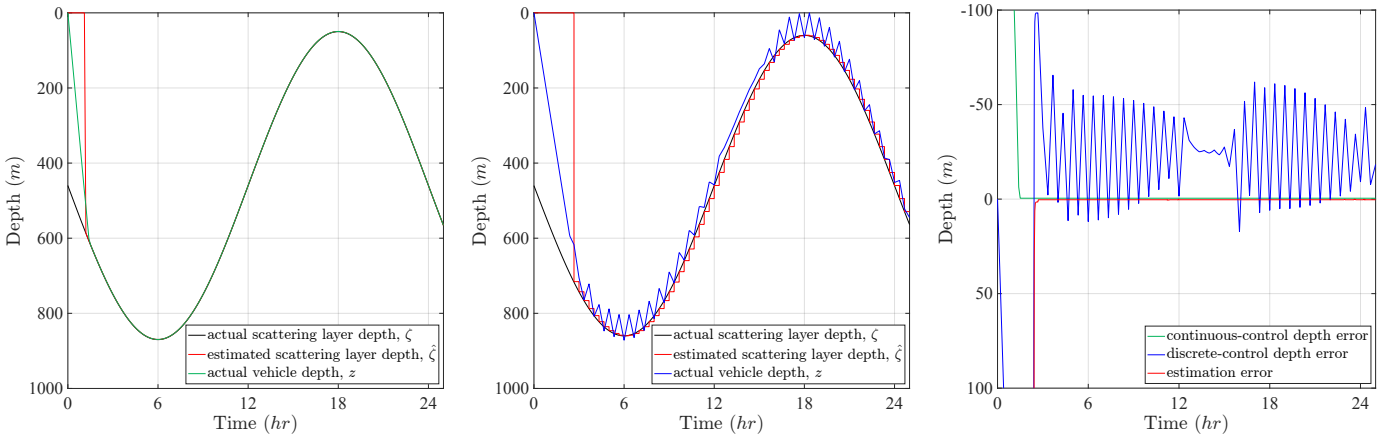

Fig. 4. Simulated output-feedback reference tracking: (a) continuous-time reference tracking; (b) discrete-time reference tracking with a 20-minute update interval; (c) tracking error

desired depth setpoint is taken to be the reference signal sampled at discrete time steps $r_k = r(t_k)$. A positive control interval T is chosen such that the time steps t_k are defined $t_{k+1} = t_k + T$ for all $t_k \geq 0$ and $k = 0, 1, \ldots$ The discrete-time error dynamics can be written in the linear form $\dot{\mathbf{e}} = (\mathbf{A} - \mathbf{BK})\mathbf{e} + \mathbf{B}\alpha$, where matrices $\mathbf{A}$ and $\mathbf{B}$ are given by (8), and α is a perturbation.

Assume $|\mu(t_k)| < \mu_{\max}$, which implies

$$\mu_k = b\dot{z}_k|\dot{z}_k| + \ddot{r}_k - K_1 e_1(t_k) - K_2 e_2(t_k), \tag{14}$$

where $\mu_k = \mu(t_k)$ and $\dot{z}_k = \dot{z}(t_k)$. Substituting (14) into (7) and using a Taylor series expansion about $e = 0$, yields

$$\begin{aligned}\dot{e}_2 = -K_1 e_1 - K_2 e_2 + b(\dot{z}_k|\dot{z}_k| - \dot{z}|\dot{z}|) - \dddot{r}\Delta t \\ + K_1 \dot{e}_1 \Delta t + K_2 \dot{e}_2 \Delta t + H.O.T.,\end{aligned} \tag{15}$$

where if Δt is sufficiently small, $\dddot{r}$ and higher order terms may be dropped. This implies

$$\dot{e}_2 = \frac{-K_1}{1 - K_2\Delta t} e_1 - \frac{K_2 - K_1\Delta t}{1 - K_2\Delta t} e_2 + \alpha, \tag{16}$$

where the perturbation term α is given by

$$\alpha = \frac{-2b\dot{z}\ddot{z}\Delta t}{1 - K_2\Delta t}. \tag{17}$$

Unlike before, the perturbation α is non-vanishing. However, it can be shown that the perturbation is bounded, which implies that the tracking error remains bounded [23]. The resulting trajectory is shown in Fig. 3b, with initial conditions $z(0) = 0$ and $r(0) = \zeta_0$, and control gains $K_1 = 0.00025$ and $K_2 = 0.275$. The depth-tracking error remains bounded for the entire integration time, as shown in Fig. 3c.

We expect the discrete-time trajectory to have larger variance about the reference signal in regions of small $\dot{r}$, and smaller variance in regions of large $\dot{r}$, as it is in the simulation results Fig. 3b. This behavior is attributed to the piecewise control that stems from the saturation function in (2), where the Driftcam ascends and descends at maximum speed to stay with the migrating layer. The areas of large error variance that occur at the deepest and shallowest points remain within the distance that a scattering layer could be observed. Additionally, having the Driftcam repeatedly cross through the layer is beneficial, as it gives more opportunities to collect data points from both above and below the nominal depth.

B. Tracking an estimated reference

Previous sections described the case where the reference signal (i.e. the scattering layer depth) is known. Here we present an estimation strategy for the scattering layer nominal depth using a dynamic observer for output-feedback control. A Luenberger observer [28] is introduced to the system to estimate the scattering layer nominal depth ζ. The observer is continuous and assumes that the output function (4) relies only on onboard measurements and calculations. The observer estimation, with Luenberger gains $\mathbf{L} = [L_1,\ L_2]^T$, is given by

$$\frac{d}{dt}\begin{bmatrix}\hat{\zeta} \\ \dot{\hat{\zeta}}\end{bmatrix} = \begin{bmatrix}\dot{\hat{\zeta}} \\ -\omega_0^2(\hat{\zeta} - \zeta_0)\end{bmatrix} + \mathbf{L}(y - \hat{y}). \tag{18}$$

The estimate of the output function (4) relies on the scattering layer state estimate $\hat{\zeta}$ and the vehicle depth z. The observer estimate converges to ζ as $t \to \infty$ for the noise-free case.

For continuous-time tracking of the scattering layer, the desired depth setpoint is taken to be the estimated scattering layer nominal depth $\hat{\zeta}(t)$ obtained in (18). The vehicle is commanded to descend until it is sufficiently close to the scattering layer to obtain a measurement. Fig. 4a demonstrates the Driftcam tracking the estimated scattering layer depth using continuous-time control with gains $K_1 = 2$ and $K_2 = 3$ and observer gains $L_1 = 1$ and $L_2 = 0$. The observer estimate converges exponentially to the expected solution given in (5).

For discrete-time tracking, the desired depth setpoints are the discrete-time samples of the estimated scattering layer nominal depth $\hat{\zeta}_k = \hat{\zeta}(t_k)$. Tracking the estimated scattering layer with discrete-time control gains $K_1 = 0.00025$ and $K_2 = 0.275$ and observer gains $L_1 = 1$ and $L_2 = 0$ is shown in Fig. 4b and Fig. 4c shows the tracking error for the Driftcam using the estimated depth as the reference signal. The Luenberger estimation is noise-free and does not take

into account measurement noise or estimation bias. The 25-meter shift in the discrete-time tracking trajectory could be resolved in future work by using an estimation strategy such as a Kalman filter.

IV. Driftcam guidance design and Results

This section presents an offboard guidance algorithm for trajectory planning for automated generation of desired depth inputs commanded to the Driftcam to track a virtual scattering layer with experimental results from laboratory and field testing. The offboard trajectory planner makes it feasible to automate the control of the Driftcam without changing the established and tested onboard firmware. The Driftcam onboard controller has been demonstrated to provide setpoint tracking in laboratory testing, as shown in Section II and previous work [7]. In simulation, we have demonstrated the capacity for the Driftcam to track the time-varying scattering layer by using a representative reference signal. To characterize the actual vehicle response to the frequent setpoint changes for the tracking behavior defined by the proposed control strategy in Section III, experimental testing is necessary. However, to avoid the time and risk of implementing a new controller onboard the Driftcam, we chose to compute the trajectory offboard and send updated commands acoustically via USBL.

A. Offboard trajectory planner design

The offboard trajectory planner uses a known time-varying reference signal and state feedback received from the vehicle to generate a new depth setpoint command and automatically send it to the Driftcam. The offboard trajectory planner is designed to emulate the autonomous reference tracking behavior discussed in Section III without altering the existing onboard controller. The diagram in Fig. 5 shows the flow of

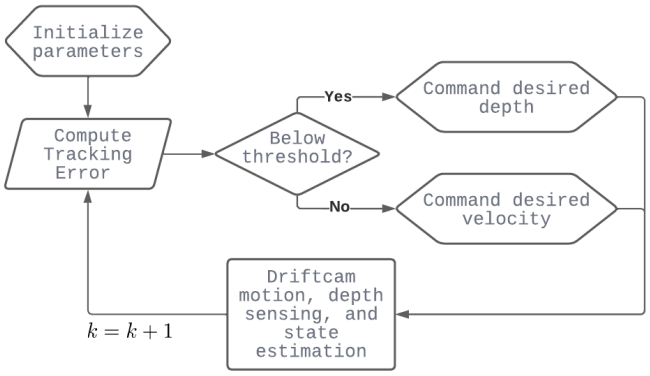

Fig. 5. Diagram of automatic offboard trajectory planner

the trajectory planner, which is designed to be initialized at any time after the vehicle is deployed. The guidance scheme is compatible with the existing onboard PID control as well as the proposed onboard controller in Section III. The Driftcam is nominally deployed with at least one preprogrammed depth setpoint. At any point, the setpoint can be overridden by using the USBL to send a new command, setting a new depth and a maximum vertical velocity. Additional acoustic commands also allow the user to request a status response or to change the time remaining on the active mission.

Once the Driftcam is deployed, the offboard trajectory planner is initialized with the current state obtained from a status response and the scattering layer reference signal $r(t)$ is sampled at the discrete time step t_0. At each iteration t_k the tracking error is computed and used to determine whether to send a depth or velocity setpoint. If the Driftcam is within a specified margin, nominally the amplitude of the scattering layer, a depth setpoint is commanded to the onboard controller and is set as the scattering layer position. If the Driftcam is not within that margin, then the scattering layer position and length of the control interval T is used to compute a desired velocity. After sending a setpoint command, the algorithm waits until the end of the control interval and then requests a status response from the vehicle to obtain new state updates for the next iteration.

B. Experimental results

To evaluate the performance of reference tracking using the offboard trajectory planner, laboratory pool tests were conducted in May 2022 at the University of Maryland Neutral Buoyancy Research Facility and ocean tests were conducted in June 2022 at the Bermuda Institute of Ocean Sciences. Each pool test was 2 hours long, and used a control interval of 10 minutes. As with the theoretical results in Section III, the reference signal is chosen as a sinusoid representing the simple harmonic motion of the scattering layer vertical migration pattern. The sinusoid amplitude was scaled to fit in the pool and data was obtained for one oscillation period. Fig. 6a shows results from one such pool test. The Driftcam was first deployed to a depth setpoint of 4 meters and allowed to settle at depth before the trajectory planner test began. This procedure was performed to allow the onboard volume controller and engine to get balanced properly. When the Driftcam is first put in the water the engine is initialized to be neutrally buoyant. The engine volume controller must compensate for nonlinear effects such as trapped air in the vehicle frame requiring about 3 minutes for the vehicle's depth to converge on the setpoint, as seen in the beginning of Fig. 2.

The Bermuda ocean trial had a control interval of 5 minutes and was 47 minutes long, limited by availability of the boat and crew. The reference sinusoid was scaled such that the Driftcam would remain in the water column in shallow-water conditions and had an oscillation period of 40 minutes. Results from the ocean test are shown in Fig. 6b. Prior to this trial, the depth control system was tuned to operate at a target depth greater than 20 meters. Within the first 20 meters a mixing layer occurs, which often yields very little change in seawater density with respect to depth. Trapped air, however, will rapidly increase the density of the platform with respect to depth near the surface following the ideal gas law, making depth control unstable near the surface. Typically below 50 meters, a strong density seawater gradient (or pycnocline) occurs, which yields natural stability for density-based depth control while the density variation in the platform due to trapped air with respect to depth is negligible. The Driftcam

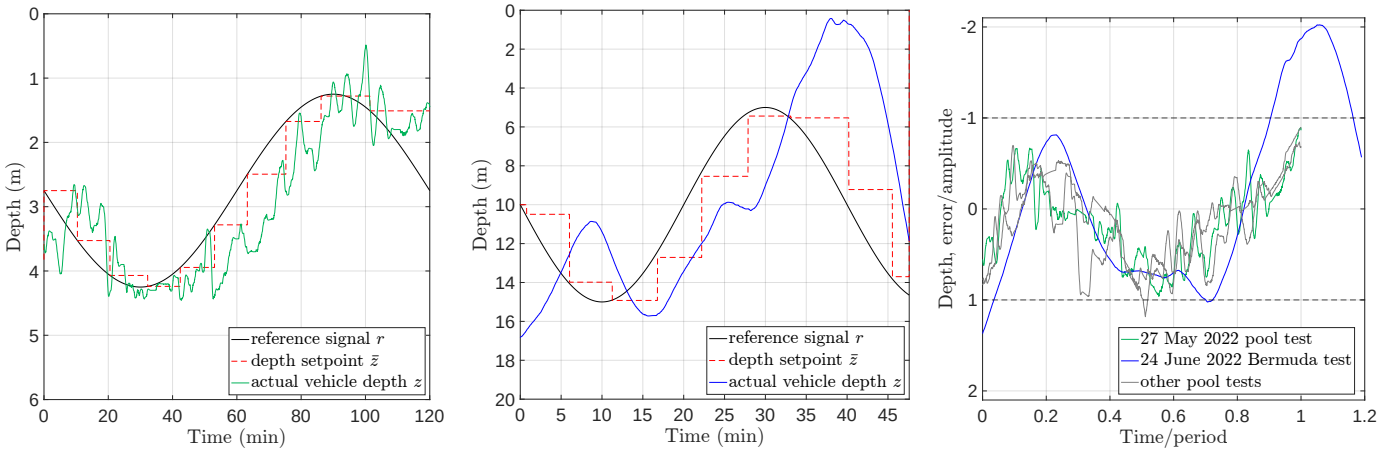

Fig. 6. Experimental results of automated offboard trajectory planner in: (a) 27 May 2022 pool test, discrete control interval T=10 minutes, sinusoid period 120 minutes, amplitude 1.5 meters; (b) 24 June 2022 ocean test, discrete control interval T=5 minutes, sinusoid period 40 minutes, amplitude 5 meters; (c) tracking error comparison

controller was initially tuned to operate at depths greater than 100 meters in open ocean testing. It should be noted that a volume correction was incorporated into the depth control system to account for trapped air to enable pool testing, but the technique to identify the trapped air volume is tedious and not practical for open ocean testing. Fig. 6c shows the tracking error of the tests combined into one axis. For each test the time vector and depth error are normalized by the reference period and amplitude, respectively.

TABLE I
SUMMARY OF RESULTS, BOLD SHOWN IN FIG. 6

Date	Location	Mean depth (m)	Amplitude (m)	RMSE (m)
27 May	Pool	2.75	1.5	0.6610
30 May	Pool	2.75	1.5	0.7691
30 May	Pool	2.75	1.5	0.6363
24 June	Ocean	10	5	4.9698

Test results have been summarized in Table I. The offboard guidance technique was successfully demonstrated both in the laboratory and in ocean trials. Pool tests had less error than the ocean experiment. The lag between the reference signal and the actual vehicle depth in the pool and ocean tests is a result of computing the new depth setpoint as $r(t_k)$, corresponding to the beginning of the control interval. Based on the experimental results, one possible method to eliminate the lag is to compute the setpoint from the reference projected at the middle of each interval, i.e. $r(t_k + T/2)$.

In general the platform had higher stability in the pool. Conditions during pool testing were highly controlled and a feed-forward model for trapped air in the system was also utilized to correct for bubble expansion within the frame. Ocean testing was limited by available conditions and boat time. In order to improve control performance in near-surface open ocean testing, bubble-volume compensation could be applied, as it was in the pool. A future area of study that could benefit float operations near the surface is real-time compressibility parameter estimation to compensate for inherent instability near the surface. Despite these limitations, testing was performed opportunistically and showed that the testing framework and control scheme could be demonstrated in the field. Control error in open ocean testing was also well within the distance at which a scattering layer could be visually observed.

V. CONCLUSION

This work presents two complementary methods for the Driftcam to autonomously track a time-varying reference: an error-based reference tracking control strategy with theoretically proven stability and an experimentally validated trajectory-guidance algorithm. The offboard guidance scheme is compatible with the existing onboard PID controller and therefore was implemented for testing experimentally in the field. We have not yet implemented or tested the proposed onboard controller, other than in simulation, although it is fully compatible with the trajectory-guidance algorithm.

The error-based tracking strategy uses the vehicle dynamics and the target reference dynamics in a closed-loop onboard controller designed for continuous- and discrete-time control updates. The inputs to the onboard system are initial conditions and control gains; the closed-loop control minimizes depth error between the reference and vehicle trajectories. Simulation results show the system to be exponentially stable for continuous-time state- and output-feedback control, and to be stable with bounded tracking error for discrete-time state- and output-feedback control. The dynamic observer for the scattering layer depth estimate is shown to converge.

The automatic offboard trajectory-planning algorithm uses vehicle state information and the time-varying target reference to generate new depth setpoints based on state feedback from the vehicle and sends an appropriate acoustic command to change the input to the onboard controller. Since the test framework allows for a human-in-the-loop, the technique offers less risk by allowing experimental control software to be tested opportunistically at-sea. Once validated, this software could then be implemented on the target platform.

The experimental results of the trajectory planner suggest that it would be feasible for the Driftcam to implement the proposed error-based tracking strategy as an onboard depth controller for observing the migrating pelagic scattering layer. Future work could further develop the strategy for tracking an estimated reference from Section III-B by expanding the model to include added measurement noise and a Kalman filter for state estimation.

ACKNOWLEDGMENT

The authors would like to thank Charles M. Shepard, Kyler Abernathy, Tim Noyes (Bermuda Institute of Ocean Sciences), Brennan Phillips (University of Rhode Island), and Lauren Freeman (Naval Undersea Warfare Center).

REFERENCES

[1] M. D'Elia, J. D. Warren, I. Rodriguez-Pinto, T. T. Sutton, A. Cook, and K. M. Boswell, "Diel variation in the vertical distribution of deep-water scattering layers in the Gulf of Mexico," *Deep Sea Research Part I: Oceanographic Research Papers*, vol. 115, pp. 91–102, Sept. 2016.

[2] O. R. Godø, N. O. Handegard, H. I. Browman, G. J. Macaulay, S. Kaartvedt, J. Giske, E. Ona, G. Huse, and E. Johnson, "Marine ecosystem acoustics (MEA): quantifying processes in the sea at the spatio-temporal scales on which they occur," *ICES Journal of Marine Science*, vol. 71, no. 8, pp. 2357–2369, Oct. 2014. [Online]. Available: https://academic.oup.com/icesjms/article/71/8/2357/761870

[3] R. J. Milligan, A. M. Bernard, K. M. Boswell, H. D. Bracken-Grissom, M. A. D'Elia, S. DeRada, C. G. Easson, D. English, R. I. Eytan, K. A. Finnegan, *et al.*, "The application of novel research technologies by the deep pelagic nekton dynamics of the Gulf of Mexico (DEEPEND) consortium," *Marine Technology Society Journal*, vol. 52, no. 6, pp. 81–86, 2018.

[4] E. G. Barham, "Deep scattering layer migration and composition: observations from a diving saucer," *Science*, vol. 151, no. 3716, pp. 1399–1403, 1966.

[5] E. J. Berkenpas, B. S. Henning, C. M. Shepard, A. J. Turchik, C. J. Robinson, E. J. Portner, D. H. Li, P. C. Daniel, and W. F. Gilly, "A buoyancy-controlled Lagrangian camera platform for in situ imaging of marine organisms in midwater scattering layers," *IEEE Journal of Oceanic Engineering*, vol. 43, no. 3, pp. 595–607, July 2018. [Online]. Available: https://ieeexplore.ieee.org/document/8026568/

[6] P. C. Davison, J. A. Koslow, and R. J. Kloser, "Acoustic biomass estimation of mesopelagic fish: backscattering from individuals, populations, and communities," *ICES Journal of Marine Science*, vol. 72, no. 5, pp. 1413–1424, 2015.

[7] E. J. Berkenpas, C. M. Shepard, R. J. Suitor, P. Zaidins, D. A. Paley, and K. Abernathy, "Swarming Driftcams: a novel platform for locating and tracking pelagic scattering layers," in *OCEANS 2021: San Diego - Porto*, San Diego, CA, 2021, pp. 1–6.

[8] J. Lee, B. Free, S. Santana, and D. A. Paley, "State-feedback control of an internal rotor for propelling and steering a flexible fish-inspired underwater vehicle," in *2019 American Control Conference (ACC)*. Philadelphia, PA, USA: IEEE, July 2019, pp. 2011–2016. [Online]. Available: https://ieeexplore.ieee.org/document/8814908/

[9] J. Boehm, E. Berkenpas, C. Shepard, and D. A. Paley, "Feedback-linearizing control for velocity and attitude tracking of an ROV with thruster dynamics containing input dead zones," in *2019 American Control Conference (ACC)*, 2019, pp. 5699–5704.

[10] W. Kohnen, "Review of deep ocean manned submersible activity in 2013," *Marine Technology Society Journal*, vol. 47, no. 5, 2013.

[11] B. H. Robison, "Deep pelagic biology," *Journal of experimental marine biology and ecology*, vol. 300, no. 1-2, pp. 253–272, 2004.

[12] R. Capocci, G. Dooly, E. Omerdić, J. Coleman, T. Newe, and D. Toal, "Inspection-class remotely operated vehicles — A review," *Journal of Marine Science and Engineering*, vol. 5, no. 1, p. 13, 2017.

[13] R. D. Christ and R. L. Wernli Sr, *The ROV manual: a user guide for remotely operated vehicles*. Butterworth-Heinemann, 2013.

[14] K. Raskoff, R. Hopcroft, K. Kosobokova, J. Purcell, and M. Youngbluth, "Jellies under ice: ROV observations from the Arctic 2005 hidden ocean expedition," *Deep Sea Research Part II: Topical Studies in Oceanography*, vol. 57, no. 1-2, pp. 111–126, 2010.

[15] P. G. Fernandes, P. Stevenson, A. S. Brierley, F. Armstrong, and E. J. Simmonds, "Autonomous underwater vehicles: future platforms for fisheries acoustics," *ICES Journal of Marine Science*, vol. 60, no. 3, pp. 684–691, 2003.

[16] N. Carter, *Autonomous Underwater Vehicles: Technology and Applications*. Clanrye International, 2015.

[17] T. Dickey, E. C. Itsweire, M. Moline, and M. Perry, "Introduction to the Limnology and Oceanography special issue on autonomous and Lagrangian platforms and sensors (ALPS)," *Limnology and Oceanography*, vol. 53, no. 5part2, pp. 2057–2061, 2008.

[18] D. R. Yoerger, A. F. Govindarajan, J. C. Howland, J. K. Llopiz, P. H. Wiebe, M. Curran, J. Fujii, D. Gomez-Ibanez, K. Katija, B. H. Robison, *et al.*, "A hybrid underwater robot for multidisciplinary investigation of the ocean twilight zone," *Science Robotics*, vol. 6, no. 55, p. eabe1901, 2021.

[19] X. André, P.-Y. Le Traon, S. Le Reste, V. Dutreuil, E. Leymarie, D. Malardé, C. Marec, J. Sagot, M. Amice, M. Babin, *et al.*, "Preparing the new phase of Argo: technological developments on profiling floats in the NAOS project," *Frontiers in Marine Science*, vol. 7, p. 577446, 2020.

[20] C. Roman, G. Inglis, and B. McGilvray, "Lagrangian floats as sea floor imaging platforms," *Continental Shelf Research*, vol. 31, no. 15, pp. 1592–1598, 2011.

[21] N. E. Leonard, "Stability of a bottom-heavy underwater vehicle," *Automatica*, vol. 33, no. 3, pp. 331–346, Mar. 1997. [Online]. Available: https://www.sciencedirect.com/science/article/pii/S0005109896001768

[22] N. E. Leonard and J. E. Marsden, "Stability and drift of underwater vehicle dynamics: mechanical systems with rigid motion symmetry," *Physica D: Nonlinear Phenomena*, vol. 105, no. 1-3, pp. 130–162, 1997.

[23] H. K. Khalil, *Nonlinear Systems*, 3rd ed. Upper Saddle River, NJ, USA: Prentice Hall, 2002.

[24] S. Le Reste, V. Dutreuil, X. André, V. Thierry, C. Renaut, P.-Y. Le Traon, and G. Maze, ""deep-Arvor": A new profiling float to extend the Argo observations down to 4000-m depth," *Journal of Atmospheric and Oceanic Technology*, vol. 33, no. 5, pp. 1039–1055, 2016.

[25] N. Fofonoff and R. Millard Jr, "Algorithms for computation of fundamental properties of seawater," *Unesco Technical Papers in Marine Science*, vol. 44, pp. 25–28, 1983.

[26] D. E. Cade and K. J. Benoit-Bird, "Depths, migration rates and environmental associations of acoustic scattering layers in the Gulf of California," *Deep Sea Research Part I: Oceanographic Research Papers*, vol. 102, pp. 78–89, 2015.

[27] T. I. Fossen, *Handbook of marine craft hydrodynamics and motion control*. Chichester, West Sussex: Wiley, 2011.

[28] J. P. Hespanha, *Linear systems theory*. Princeton University Press, 2018.